High Performance Multicell Series Inverter-Fed Induction Motor Drive

[1]M. Khodja, [2]D. Rahiel, [3]M.B. Benabdallah, [1,3]H.Merabet Boulouiha, [3]A. Allali, [2]A. Chaker, [4]M. Denai

[1]*Centre universitaire de Relizane Ahmed Zabana CUR-AZ, Algérie*

[2]*Ecole Normale Polytechnique d'Oran ENPO, Algérie*

[3]*Faculté de Génie Electrique, Département d'Electrotechnique*

LDDEE, Laboratoire de Développement Durable de l'Energie Electrique

Université des Sciences et de la Technologie d'Oran,

[4]*School of Engineering & Technology, University of Hertfordshire, Hatfield AL10 9AB, UK*

khodja1970@gmail.com, rahiel_djelloul@yahoo.fr, benabdallah22@yahoo.fr, houari.merabet@gmail.com, allalia@yahoo.com, chakeraa@yahoo.fr, m.denai@herts.ac.uk

Abstract - The multilevel voltage-source inverter (VSI) topology of the series multicell converter developed in recent years has led to improved converter performance in terms of power density and efficiency. This converter reduces the voltage constraints between all cells, which results in a lower transmission losses, high switching frequencies and the improvement of the output voltage waveforms. This paper proposes an improved topology of the series multicell inverter which minimises harmonics, reduces torque ripples and losses in a variable speed induction motor drive. The flying capacitor multilevel inverter topology based on the classical and modified phase shift pulse width modulation (PSPWM & MPSPWM) techniques are applied in this paper to minimise harmonic distortion at the inverter output. Simulation results are presented for a 2 kW induction motor drive and the results obtained demonstrate reduced harmonics, improved transient responses and reference tracking performance of the voltage in the induction motor and consequently reduced torque ripples.

Keywords: Multicell converter, induction machine, phase-shift PWM, indirect vector control, fuzzy logic control.

1. Introduction

Many variable speed induction motor drive applications require high torque dynamics and low torque ripples to meet the requirements of high productivity and improved accuracy. In commercial variable speed induction motor drives, two control schemes based on field-oriented control (FOC) [1-3] and direct torque control (DTC) [4] have been widely for more than two decades.

DTC [5,6] has proved to be a very effective method for the control of induction machines. As compared to field oriented control (FOC), DTC implementation minimises the use of machine parameters [7,8] while maintaining the advantages of fast transient response characteristics. Nevertheless, these two control techniques have a major disadvantage as they exhibit ripples at high torque and flux values which also results in high acoustic noise [9].

In the early 90s, a new structure of multilevel converters has been proposed [10-11]. This structure is based on the series connection of switching cells between which a floating voltage source is inserted. These floating voltage sources are realized with capacitors. The series multicell structure can be adapted to all types of configurations including chopper or inverter with a capacitive medium point, half bridge or full bridge.

Multilevel inverters are becoming essential to achieve high quality output voltages with a substantial reduction in the THD (Total Harmonic Distortion). The overall size of the converter is also reduced and consequently these converter types are becoming very popular and are being used in a wide range of industrial applications in recent years [12-24].

In [25], a sliding mode control (SMC) based on indirect field oriented control (IFOC) was applied to control the speed of an induction motor using a dSPACE DS1104 interface card.

A medium voltage five-level NPC (Neutral Point Clamped) inverter-fed induction motor for industrial applications has been studied in [26-27]. The inverter is supplied by a Z-type source to provide more flexibility for the DC current. The induction motor control is based on DTC. A comparative study between a conventional PI (proportional-integral) and fuzzy logic control (FLC) of the induction motor has been studied in [28]. In [29], model predictive control (MPC) is applied to a multicell converter. The control strategy has been tested both in simulations using Matlab/Simulink and validated experimentally using a dSPACE card.

A comparative study of three DTC control methods for a squirrel cage induction generator (SCIG) was presented in [30]. Namely, the classical DTC, the DTC-SVPWM fixed frequency inverter with two level and three-level NPC topologies. The switches are controlled by three-level SVPWM which takes into consideration the balancing the DC link voltage.

In this paper, rotor flux oriented vector control of the induction motor based on a series multicell converter is proposed to improve the quality of the three-phase currents and consequently minimising torque ripples.

This paper is organized as follows: Section 2 describes the topology of the flying capacitor multilevel inverter (FCMI) driving an induction motor and presents the generalized switching law for FCMI based on the phase-shifted PWM (PSPWM) strategy. Section 3 describes the arrangement for a general simulation model and develops the control design of the induction motor based on indirect field oriented control (IFOC) using both a classical PI and FLC controllers. Section 4 presents the control strategy of the switching based on PSPWM technique. The simulation results for the conventional and multicell inverters topologies controlled respectively by PI and FLC controllers are presented in the Section 5. Finally, conclusions and future perspectives are discussed in Section 6.

2. Structure and Control Scheme of the Multicell Inverter Fed Induction Motor Drive

The power circuit of the variable speed induction motor drive considered in this paper is presented in Fig. 1.

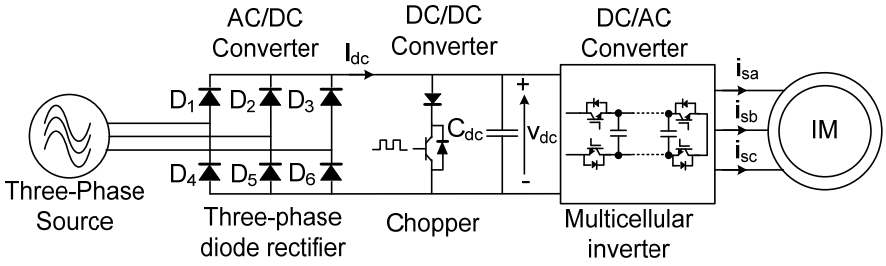

Fig. 1 Power circuit of the multicellular inverter induction motor drive

2.1 Overview of the multicell converter

The type of converter selected in this paper is the multi-serial converter based on the so-called Meynard & Foch structure which results from the connection of N floating voltage sources in series to obtain $(N+1)$ discrete

levels of output voltage, indexed from 0 to N (noted n). The voltage sources are the voltage of the power bus (constant voltage) v_{dc} and the $(N-1)$ capacitors used as foating sources.

With the symmetric PWM control, this structure has the following properties: (i) natural stability, (ii) minimum number of commutations (only two per cell in a period), (iii) low harmonic level, (iv) voltage constraints equally distributed on each switch. However, in order to analyse the properties of multicell series converter in steady state, the following assumptions are made to simplify the study: (i) the switches are supposed ideal, (ii) the dead-time will be taken equal to zero and (iii) the voltage and current sources are assumed ideal.

The general scheme for three-phase multicell converter associated with an induction motor is illustrated in Fig. 2.

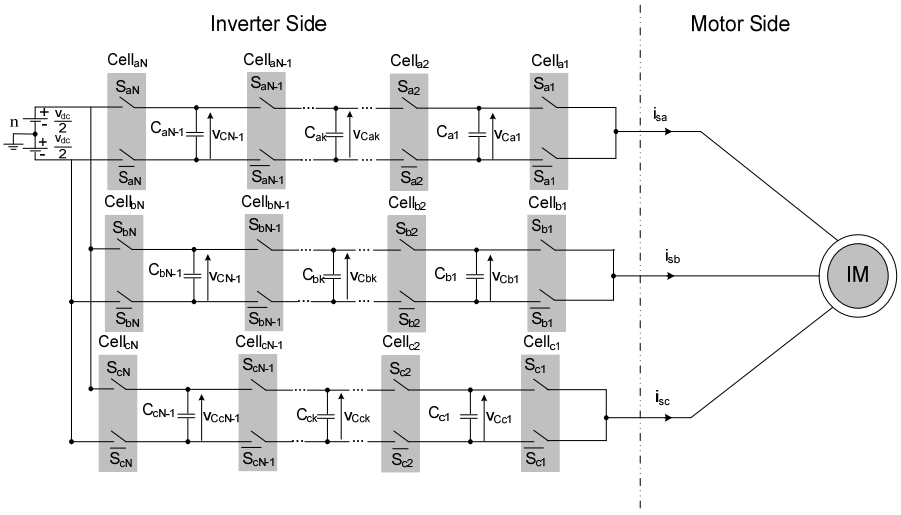

Fig. 2 Structure of the multilevel inverter with N cells connected to the induction motor.

The multilevel inverter consists of pairs of semiconductor switches separated by floating capacitors. The two switches in each pair must always be complementary in order to avoid shorting the voltage sources. Each pair of switches represents a switching cell. The principle of this topology is to divide the DC bus voltage into several basic voltage sources. The operation of each switching cell is similar to a two-level inverter with a voltage source equal to v_{dc}/N (N is the number of cells and v_{dc} is the supply voltage) and a current source. The maximum voltage of the IGBTs switching are achieved by $V_{max} = v_{dc}/N$.

The first advantage of these converters is the reduced voltage requirements on the switches. It is necessary to identify all the converter possible states, the voltage across the floating capacitors and the converter's output voltage level for all states (equal to $jv_{dc}/N, j = 1, \cdots N$). Multicell series converters also improve the waveform of the output voltage and allow greater flexibility for different voltage levels as compared to the NPC structure.

This study focuses on a three phase five-level multicell inverter topology to highlight the following two results:

(i) Increased voltage levels: By increasing the level of the structure, the stress on the IGBTs can be reduced, consequently the multicell inverter provides more levels than the NPC or cascade inverter topologies.

(ii) Increased bandwidth: The multicell inverter allows an increase in the harmonics switching frequency [31] in proportion with the number of cells. Hence the harmonics will be shifted farther from the fundamental.

2.2 PSPWM switching control

The PSPWM control is based on a frequency behavior of the converter. The main idea is to achieve N binary signal with identical phase shift of $2\pi/N$. The duty cycle of these signals is calculated in order to adjust the output

current in order to control the speed of the induction motor. The switching between modes generates a harmonic in the current. The capacitor voltages are naturally balanced around their baseline values. The PWM control is usually generated by comparing a triangular and reference signals. In PSPWM, a sinusoidal reference voltage waveform is compared with a triangular carrier signal to generate the gate signals for controlling the switches of multicell-inverter. The PSPWM control method leads to reduced switching losses. Note that it is possible to obtain N different switching cycles.

The control of the multicell inverter is obtained by a PSPWM strategy. When all the cells are controlled with a square wave signal, the following results are obtained:

- With an the same phase shift between adjacent cells, the output voltage uses simply two levels and the harmonics are multiples orders of Nf_c (f_c being the switching frequency), then the offset is:

$$\varphi = \frac{2\pi}{N} \tag{1}$$

- With equal amplitude modulation indices M_i in all three phases, the output voltage fundamental of V_{s1} does not depend on the state of the inverter, but only on the bus voltage and modulation index:

$$V_{s1} = M_i \times v_{dc} \tag{2}$$

For optimal operation, the control signals must have the same phase shift of $2\pi/N$. There are several solutions to achieve this and in this paper a simple method is presented.

In the classical PWM, the control signal for each cell is generated by the intersection between a triangular carrier frequency f_p and the modulating sinusoidal signal of frequency f_m. The equations to generate triangular signals noted t_{rk} evolving on the interval [-1,1] are:

$$\begin{aligned}
t_{r1} &= \frac{1}{2}\left[1 + \frac{2}{\pi}\sin^{-1}\left(\sin\left(2\pi f_p t - \varphi_1 + \frac{\pi}{2}\right)\right)\right] \\
t_{r2} &= \frac{1}{2}\left[1 + \frac{2}{\pi}\sin^{-1}\left(\sin\left(2\pi f_p t - \varphi_2 + \frac{\pi}{2}\right)\right)\right] \\
t_{r3} &= \frac{1}{2}\left[1 + \frac{2}{\pi}\sin^{-1}\left(\sin\left(2\pi f_p t - \varphi_3 + \frac{\pi}{2}\right)\right)\right] \\
&\vdots \\
t_{rN} &= \frac{1}{2}\left[1 + \frac{2}{\pi}\sin^{-1}\left(\sin\left(2\pi f_p t - \varphi_N + \frac{\pi}{2}\right)\right)\right]
\end{aligned} \tag{3}$$

By generalizing equation (3) yields:

$$t_{rk} = \frac{1}{2}\left[1 + \frac{2}{\pi}\sin^{-1}\left(\sin\left(2\pi f_p t - \varphi_{ik} + \frac{\pi}{2}\right)\right)\right] \tag{4}$$

Where

$$\varphi_{ik} = (k-1)\frac{2\pi}{N} \tag{5}$$

2.3 Modified PSPWM

In three phase, harmonics can be reduced without reducing the amplitude of the output voltage because the harmonic of order 3 or a multiple of 3 are eliminated from the output voltages. A harmonic of order 3 can be added to a sinusoid of frequency f_m to form the reference waveform. This harmonic appears in the three fictitious voltages V_{ao}, V_{b0} and V_{c0} with respect to the fictitious mid-point 0, but does not appear in the phase output voltages V_{an}, V_{bn}, V_{cn} and line-to-line output voltages V_{ab}, V_{bc}, V_{ca}.

The addition of harmonic of order 3 increases the maximum amplitude of the fundamental in the output voltages. Fig. 3 shows that the reference voltage is composed of two sinusoids one for the fundamental and the other for the harmonic of order 3.

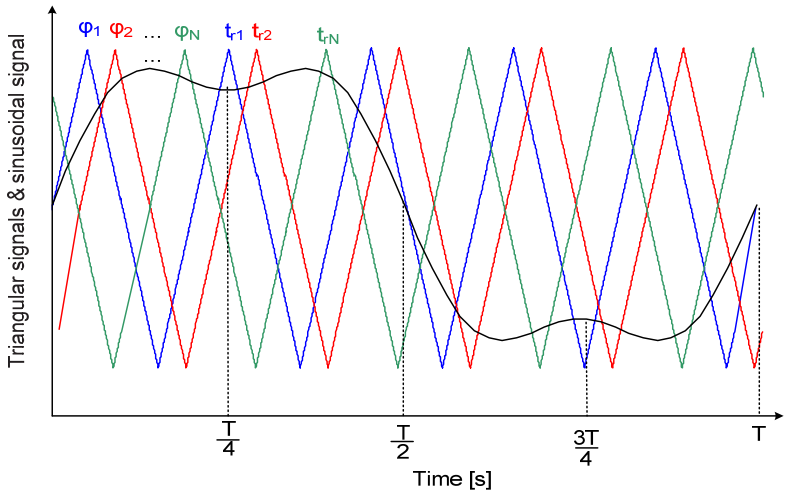

Fig. 3 Sub-optimal PSPWM.

The new reference signal for the modified PSPWM is:

$$(V_a - V_o)_w = \frac{U}{2}\left(M_i\, sin(\omega t) + k\, sin(3\omega t)\right) \tag{6}$$

This is called sub-optimal control.

The maximum value of M_i occurs for $k = 1/3\sqrt{3}$ and is found as:

$$M_{i_{max}} = \frac{2}{\sqrt{3}} \tag{7}$$

Therefore, with sub-optimal control, the maximum amplitude of the fundamental output voltage V_1 corresponding to $M_{i_{max}}$ is:

$$V_{1,M_{i_{max}}} = 2/\sqrt{3}\, V_{dc} \tag{8}$$

The basic principle of the conventional intersective modulation can directly be used to control a cell with series switches (Fig. 4). The classical and modified PSPWM provide the control (variable t_{ON}) as shown in Fig. 4 which is illustrated for a switching frequency $f_p = 600\, Hz$.

For example, consider a three-phase inverter with three-cells ($N = 3$) with the following parameters: $v_{dc} = 400\, V, L_L = 20\, mH, R_L = 0.5\, \Omega, f_m = 50\, Hz, f_p = 600\, Hz, M_i = 0.8$.

In steady state, the C_1 and C_2 capacitor voltages reached balanced values of 133.33 V and 266.66 V respectively (this is a natural balancing). From the simulation results, the following remarks can be drawn:

1) If the control signals of the switching cells have the same modulation index in magnitude and are phase shifted by $2\pi/N$ (for this simulation $N = 3$ as shown in Fig. 5) then there is only one open-loop stable state for the distribution capacitors voltages: $v_{C_j} = \frac{j\, v_{dc}}{N}$ (avec $N = 3$) and $j = 1 \cdots (N-1)$.

2) From Fig. 5, the following points can be drawn: The maximum theoretical fundamental voltage is $\frac{M_i v_{dc}\sqrt{3}}{2} = \frac{0.8\times400\times\sqrt{3}}{2} = 277.1281V$ V which is close to the value obtained 276.9 V in the simulation. The spectral analysis shows that Fourier harmonics are rejected to the higher order frequency $N \times f_p = 3 \times 600 = 1800\ Hz$ which improves the quality of three-phase currents and facilitates filtering.

3) From Fig. 5, the following remarks can be drawn: (i) the instantaneous line-to-line voltage contains three voltage levels in addition to level zero hence four levels in total, (ii) the theoretical fundamental peak voltage is $\frac{M_i v_{dc}\sqrt{3}}{2} = \frac{0.8\times400\times\sqrt{3}}{2} = 277.1281V$ which is close to the value obtained in the simulation, (iii) Fourier spectral analysis has shown that harmonics are rejected towards high frequencies of order $N \times \frac{f_{swit}}{f_m} = 3\frac{600}{50} = 36$ (corresponding to a frequency of 600 × 3 = 1800 Hz. This will improve the quality of the three-phase currents and make the filtering of these harmonics easier.

4) The harmonic spectrum of the line-to-line output voltage of phase A of the multicell are shown in Fig. 5. From this Figure, the THD is 43.60 % for the classical PSPWM and 37.40 % for proposed PSPWM. In this case, the group of harmonics can be shifted further away from the fundamental frequency. This leads to a good quality of the currents at the output of the inverter.

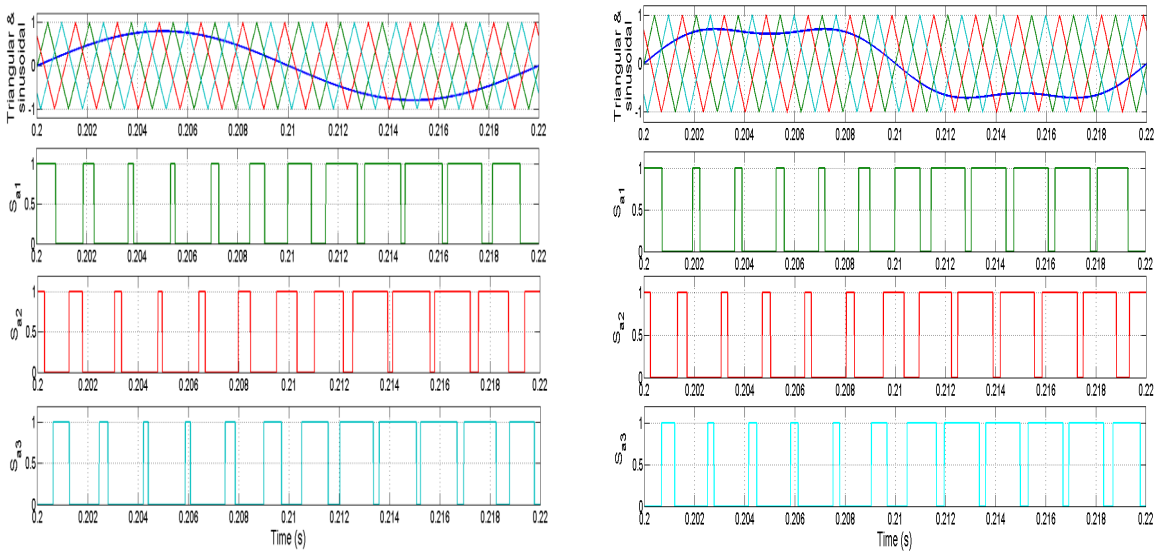

(a) (b)

Fig. 4 PSPWM strategy applied to the multicell inverter
(a) Classical PSPWM (b) Modified PSPWM

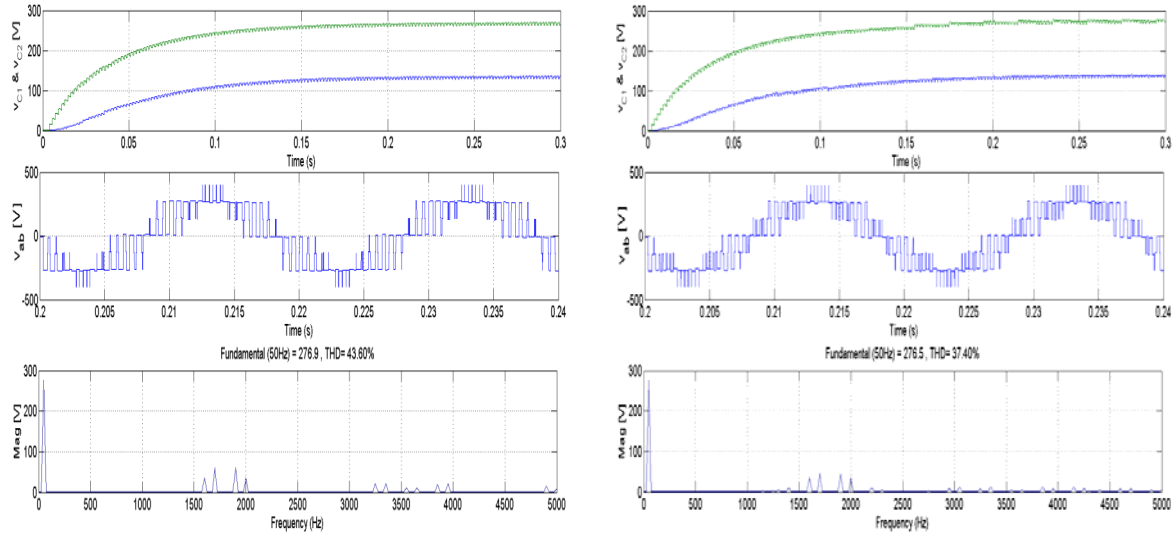

(a) (b)

Fig. 5 Waveforms of the capacitors voltages, line-to-line output voltage and its harmonic spectrum
(a) Classical PSPWM (b) Modified PSPWM

3. Indirect Vector Control of the Multicell-Fed Induction Motor Drive

This method is based on the estimation of the position of the flux vector. The voltages or currents ensuring the orientation of the flux and decoupling are estimated from a dynamic model of the machine. It is important to note that the indirect method is simpler to implement and widely used than the direct method, but the choice between the two methods vary from one application to another. Fig. 6 illustrates the principle of the indirect rotor flux oriented control (IFOC) of a variable speed induction motor drive.

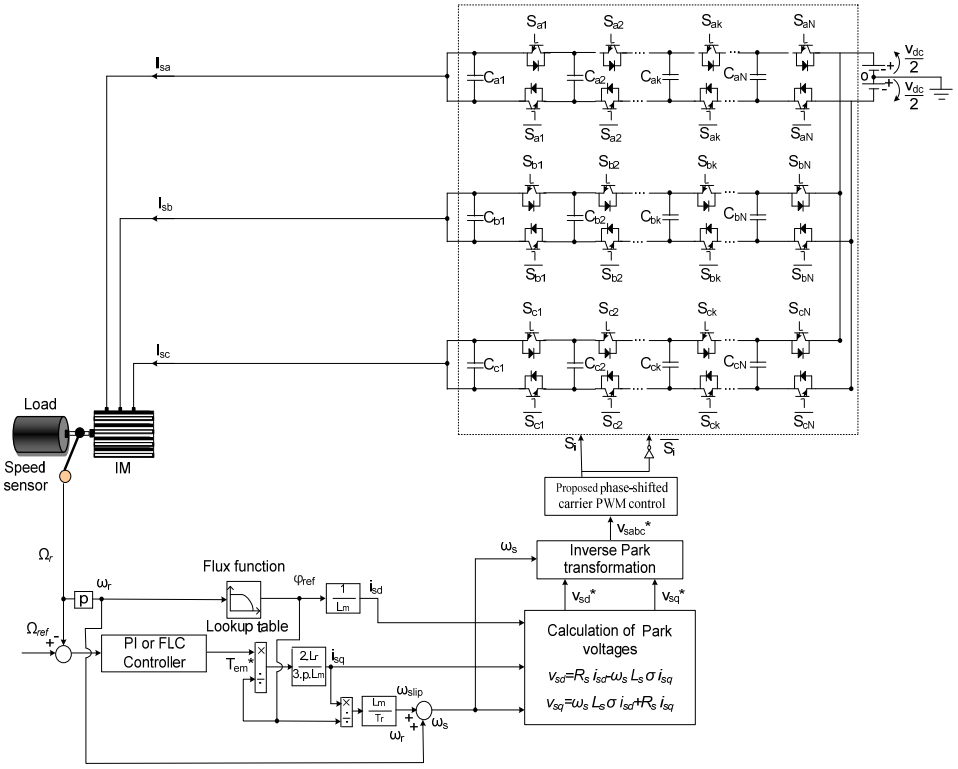

Fig. 6 Bloc diagram of IFOC for the multicell inverter-fed induction motor.

The IFOC control block generates the three-control variables v_{sd}, v_{sq} and ω_m, according to two reference inputs (i_{sq}, φ_{ref}) that ensure decoupling. These control quantities generated by the IFOC block are used to adjust the direct i_{sd} and quadratic i_{sq} components of the stator currents to their reference values, and therefore the flux and torque are maintained at their reference values. In our case, the voltages or currents provide the direction of the flux and the decoupling. An electrical model of the machine is required to develop the algorithms necessary for defining v_{sd} and v_{sq} control variables.

The strategy of indirect vector control of the induction motor was based on a classical PI control designed using a pole placement technique. The stator flux is maintained at its rated value (φ_{sn}) for the system to operate in the range of the base speed. For speeds higher than the base speed, the flux cannot be maintained constant; it must be reduced to limit the voltage at the machine terminals. Under these conditions, the reference flux is defined by:

$$\varphi_{sref} = \begin{cases} \varphi_n & if\ |\Omega_r| \le \Omega_n \\ \dfrac{\Omega_n}{|\Omega_n|}\varphi_n & if\ |\Omega_r| > \Omega_n \end{cases} \tag{9}$$

4. Simulation results

The models for classical and multicellular inverter topologies with IFOC strategy based on the technique of SPWM, classical and modified PSPMW have been developed and implemented using Matlab/Simulink SimPowerSystems toolbox. The proposed circuit model consist of a three phase power source, the multilevel inverter and the induction motor with IFOC strategy.

The main objective of this simulation study was to analyse and compare the performance of the multicell-inverter and a conventional two-level inverter with respect to torque ripples. Different simulation scenarios are presented to evaluate the performance of the two different controllers.

A. Transient and steady-state performance

Fig. 7 and Fig. 8 show the responses of the speed, the electromagnetic torque and the stator current of phase A of the induction motor. The load torque of ± 10 N was applied. Both controllers gave satisfactory transient and steady-state tracking responses There is a small overshoot in the response produced by the PI controller.

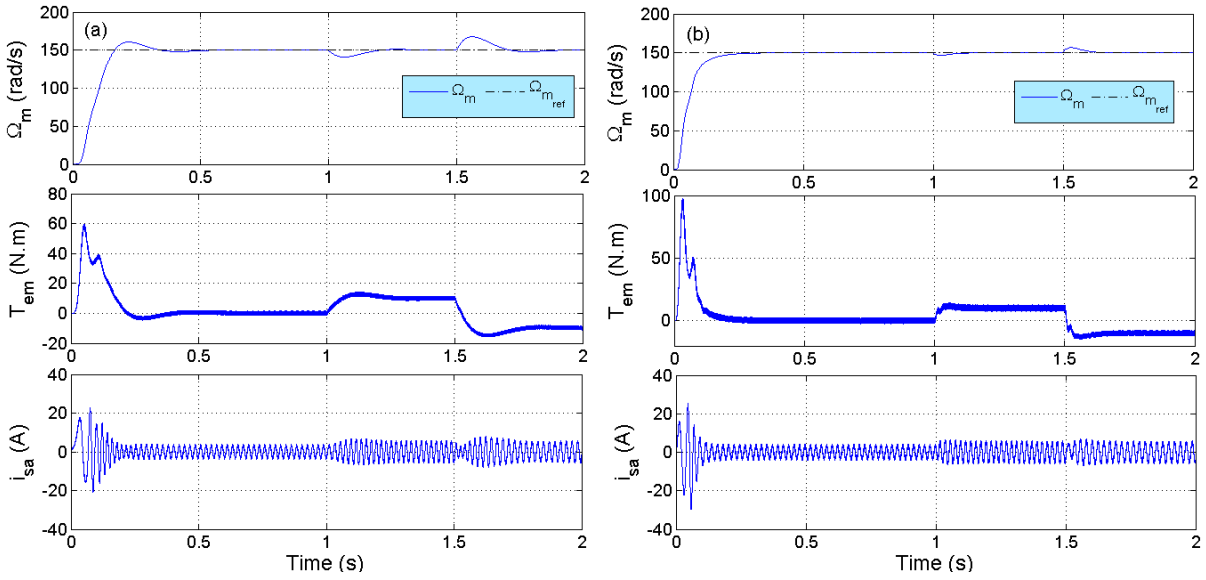

Fig. 7 Response of rotor speed, the electromagnetic torque and the stator current of phase A of the motor (a) PI controller (b) FLC.

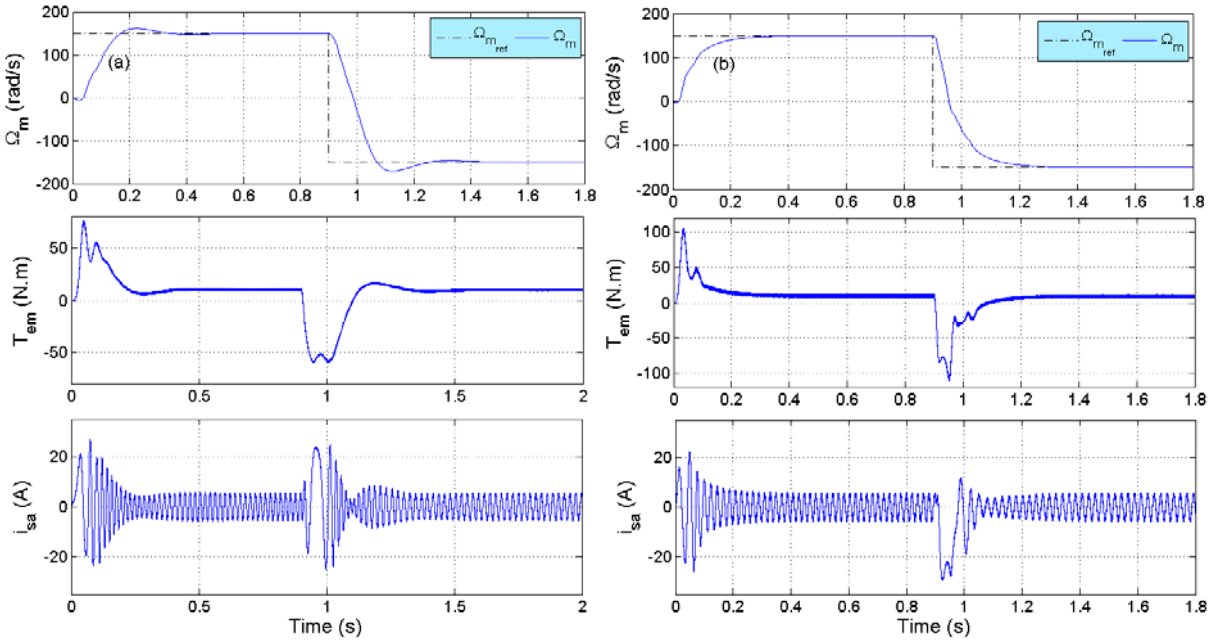

Fig. 8 Responses of rotor speed, the electromagnetic torque and the stator current of the phase A of motor with a change of reference speed by ±150 rad/s (a) PI controller (b) FLC.

B. Quality of the current and torque ripples minimisation

Electric power quality has become an important issue in recent years within the scientific and industrial communities. This concept determines the parameters that define the properties of electricity produced in normal conditions, in terms of continuity of supply and voltage characteristics (symmetry, frequency, amplitude, waveform).

Some electric equipment are considered as non-linear loads because they generate current harmonics with frequencies that are integer multiples of the fundamental frequency, or sometimes arbitrary frequencies. These harmonic currents can result in harmonic voltages at the connection points which may pollute consumers appliances connected to the same network. These harmonics also cause overload of the transmission lines, unwanted tripping, accelerated aging and performance degradation of the distribution system equipment. Consequently it necessary to reduce dominant harmonics below 5 % as specified in the IEEE harmonic standards [24].

Fig. 9 shows the responses of the rotor speed, the electromagnetic torque and the stator current of phase A of the induction motor with the conventional two-level and multicell three-level inverters. The same load torque of ± 10 N is applied to the induction motor. A significant reduction of the torque ripples has been achieved with the three-level multicell inverter as compared with the two-level inverter.

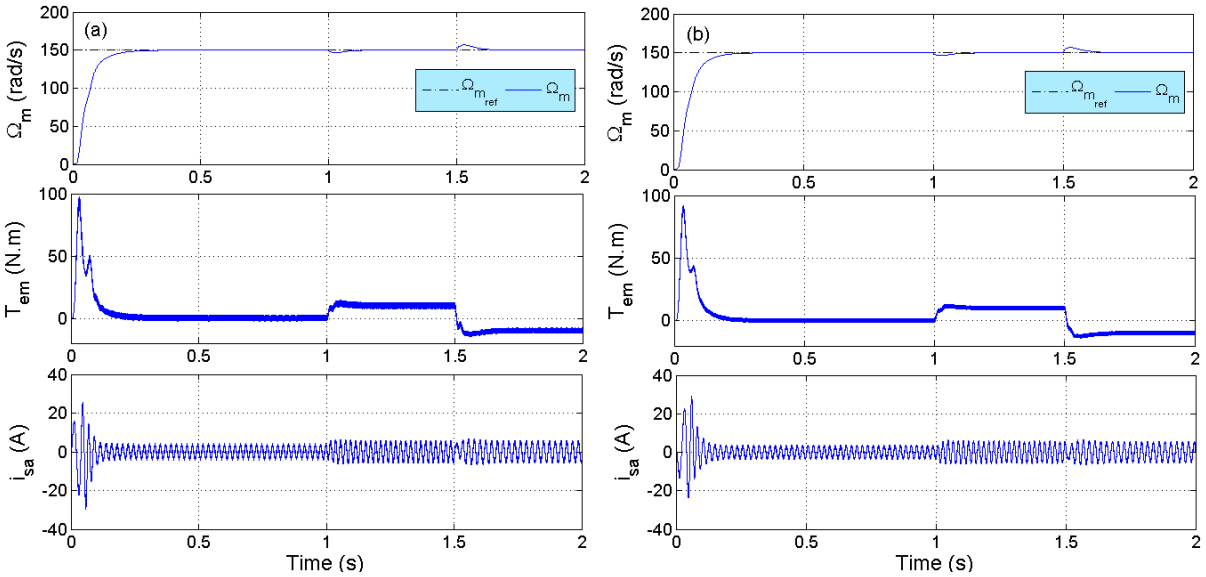

Fig. 9 Responses of rotor speed, the electromagnetic torque and the stator current of phase A of the motor (a) classical inverter (b) multicell inverter $N = 2$ (three level).

The harmonic spectrum of the current of phase A of the motor are shown in Fig.10 for the classical and multicell inverters. The THD is 5.12 % for the classical inverter and 4.44 % for three-level multicell inverter.

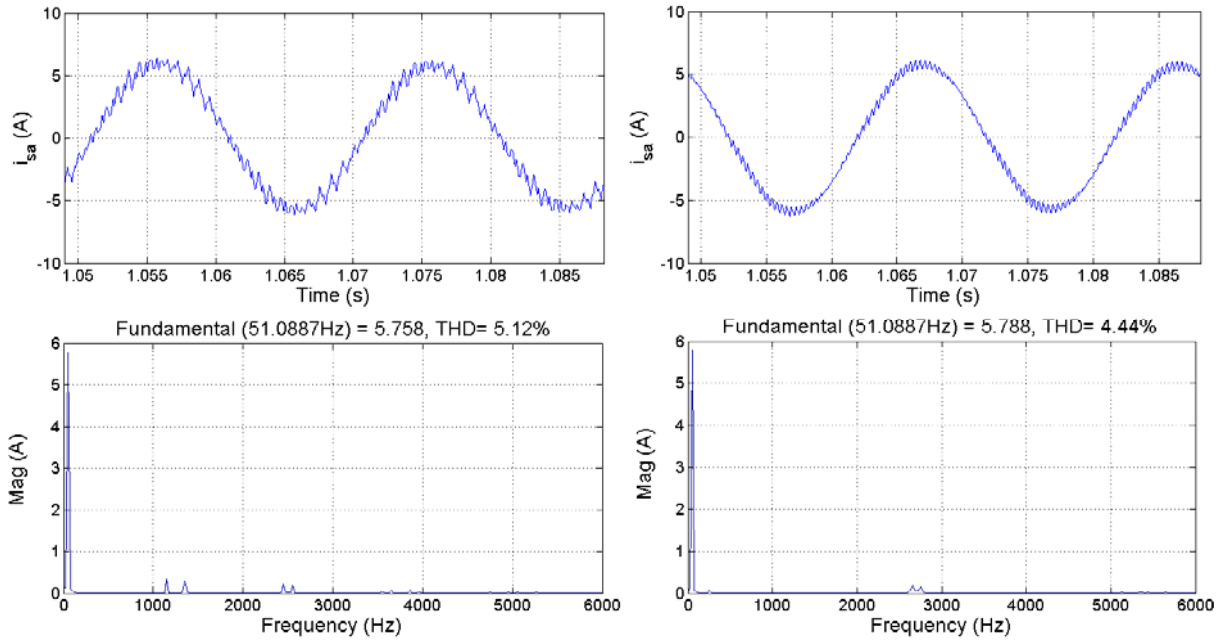

Fig. 10 Waveform of the stator current of phase A and harmonic spectrum.

(a) Classical two-level inverter (b) Multicell three-level inverter.

Fig.11 shows the response of the rotor speed, the electromagnetic torque and the stator current of phase A of the induction motor for three-, four- and five-level multicell inverter. The torque disturbance ± 10N was applied. There is a considerable reduction in the torque ripples as the number of cell is increased. These results clearly demonstrate that the five-level multicell inverter gives improved transient response and better quality of the output currents.

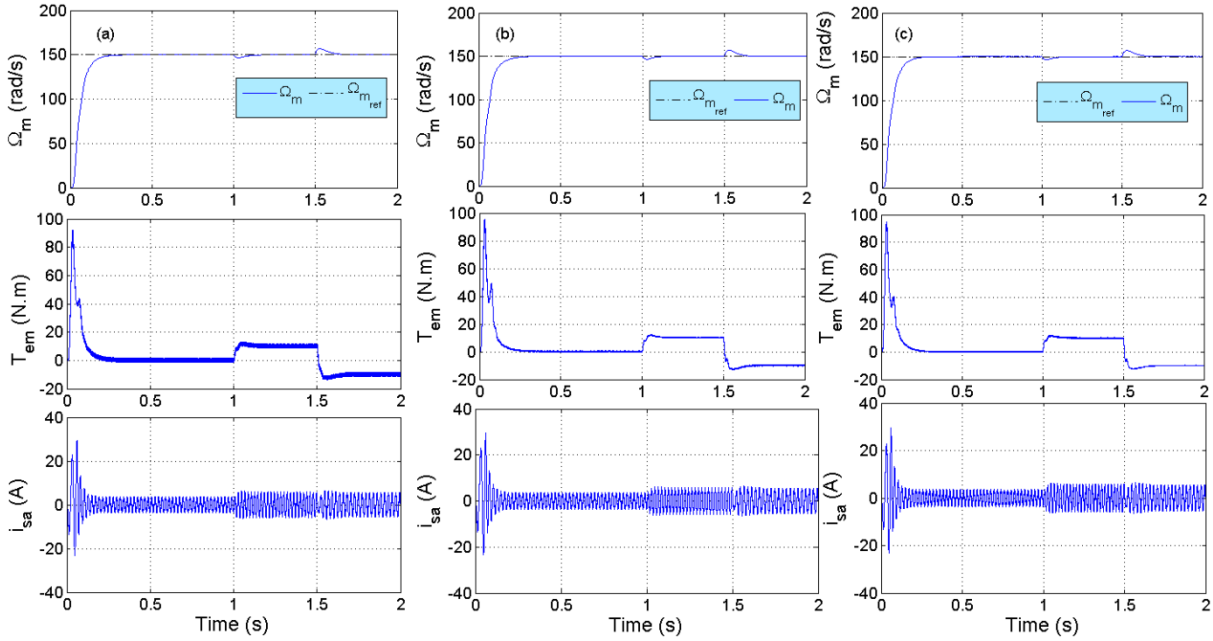

Fig. 11 Reponses of the rotor speed, electromagnetic torque and stator current the phase for the multicell inverter

(a) three-level (b) four-level (c) five-level.

The harmonic spectrum of the stator current of phase A of the motor with the three, four and five level multicell inverters respectively are shown in Fig.10.

The IEEE standards [24] are used to compare the performance of the three inverter topologies with respect to the quality of the output currents and the reduction of torque ripples. From Fig.12 and Fig.13 the following can be noted: (i) the five level multivell inverter produced the lowest THD as compared to the other converters (ii) the proposed PSPWM technique leads to the lowest THD compared to classical strategy PSPWM (iii) the five-level topology produced the lowest torque ripples and rejected harmonics towards the high frequencies.

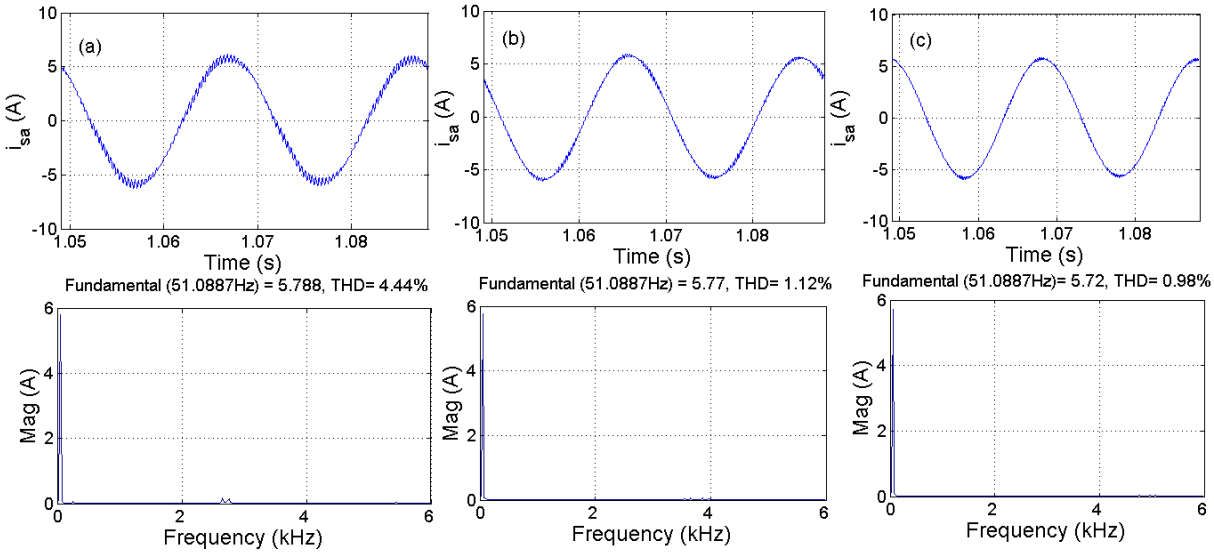

Fig. 12 Waveform of motor current of phase A and harmonic spectrum with the multicell inverter based on PSPWM (a) three level, (b) four level, (c) five level.

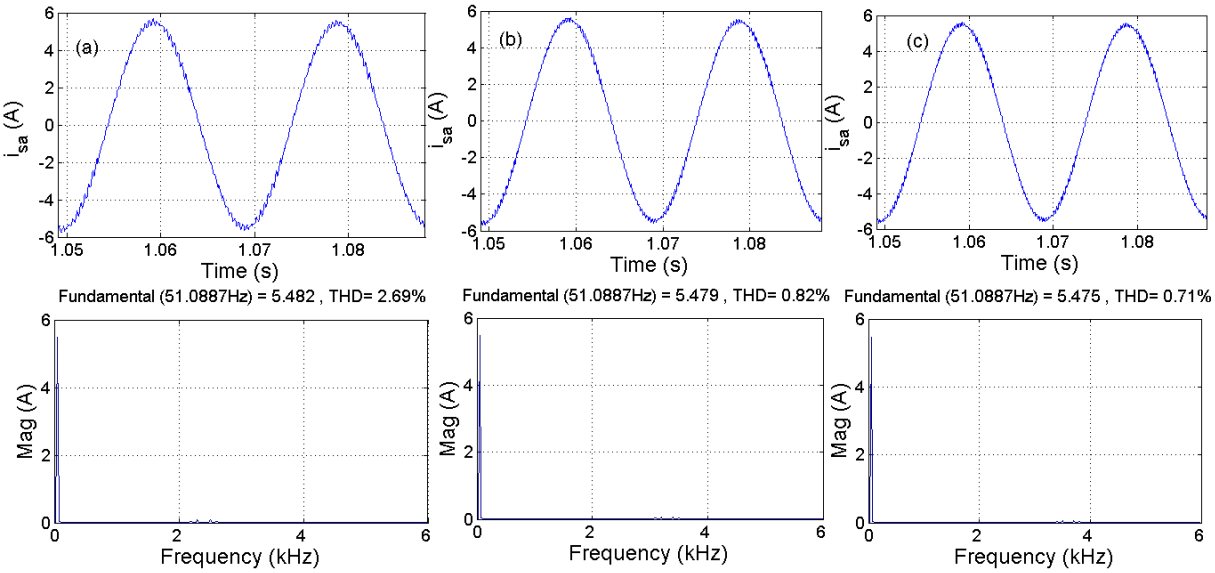

Fig. 13 Waveform of motor current of phase A and harmonic spectrum with the multicell inverter based on the modified PSPWM (a) three level, (b) four level, (c) five level.

Table 1 summarises the results and comparative performance of the inverter topologies and PWM strategies.

Table 1 Comparison of the classical inverter and multicell inverter controlled by PSPWM and the proposed PSPWM.

	Classical inverter	**Multicell inverter**					
		PSPWM			**Modified PSPWM**		
		$N = 2$	$N = 3$	$N = 4$	$N = 2$	$N = 3$	$N = 4$
THD (%)	5.12	4.44	1.12	0.98	2.69	0.82	0.71
Torque ripples (N.m)	4.12	2.8	0.8	0.5	1.45	0.62	0.27

5. Conclusion

In this paper a comprehensive simulation study of the induction motor based on the multicell-inverter topologies was presented with different control strategies to improve the quality of the current and minimise torque ripples. The indirect field oriented structure was used with the orientation of coordinate system (d, q) on the rotor to decouple the torque and flux variables. The control signals of the multicell inverter switches are achieved by a phase-shifted PWM (PSPWM) technique. The simulation results showed an enhanced performance of the induction motor transient speed response with a substantial reduction in the electromagnetic torque ripples of the induction motor. The total harmonic distortion (THD) of the stator currents of the induction motor has been reduced to 0.99% for the five levels multicell-inverter as compared to the classical inverter where the THD was 5.758% with a 1.05 kHz switching frequency. The simulation results also showed improved transient response charactersistics of the motor speed with reduced ripples using the fuzzy logic controller based on the five level multicell-inverter.

References

[1] Alkorta P., Barambones O., Garrido A. J., Garrido I, "SVPWM Variable Structure Control of Induction Motor Drives", Industrial Electronics, ISIE. IEEE International Symposium on Volume, Issue, pp.1195 – 1200, June 2007.

[2] A. Mezouar, M. K. Fellah, S. Hadjeri, 0. Touhami, Y. Sahalim**,** "Robust Direct Field Oriented Control of Induction Motors Using Adaptive Observer", IEEE ISIE 2006, July 9-12, 2006, Montreal, Quebec, Canada.

[3] S. Maiti, C. Chakraborty, S. Sengupta, Simulation studies on model reference adaptive controller based speed estimation technique for the vector controlled permanent magnet synchronous motor drive, Elsevier, Simulation Modelling Practice and Theory 17 (2009) 585–596.

[4] G. Adamidis, Z. Koutsogiannis, P. Vagdatis, Investigation of the performance of a variable-speed drive using direct torque control with space vector modulation, Electric Power Components and Systems 39 (2011) 1227–1243.

[5] Takahashi I, Noguchi T. A new quick-response and high efficiency control strategy of an induction motor. IEEE Trans Ind Appl 1986;22(5):820-7.

[6] Habetler TG, Profumo F, Pastorelli M, Tolbert Leon M. Direct torque control of induction machines using space vector modulation. IEEE Trans Ind Appl 1992;28(5):1045-53.

[7] Depenbrock M. Direct self-control of inverter fed induction machine. IEEE Trans Power Electron 1988;3(4):420-9.

[8] Habebtler TG, Divan DM. Control strategies for direct torque control of induction machines using discrete pulse modulation. IEEE Trans Ind Appl 1991;27(5):893-901.

[9] Senthil U, Fernandes BG. Hybrid space vector pulse width modulation based direct torque controlled induction motor drive. Conf IEEE. PESC'03, vol. 3; 2003. p. 1112-7.

[10] T. Meynard, H. Foch :'Milti-Level choppers for high voltage applications' EPE Journal, V.1 N°.1, 1992.

[11] T. Meynard, H. Foch, F. Forest, C. Turpin, F. Richardeau, L. Delmas, G. Gateau, E. Lefeuvre: 'Milticell converters: Derived topologies' IEEE transactions on Industrial Electronics, V.49, N°.5, pp.978-987, Special Issue on Multilevel converters, Octobre 2002.

[12] A. Ashraf Gandomi, K. Varesi, S. Hossein Hosseini : 'Control strategy applied on double flying capacitor multi-cell inverter for increasing number of generated voltage levels', IET Power Electron., 2015, Vol. 8, Iss. 6, pp. 887–897.

[13] Babaei, E., Alilu, S., Laali, S.: 'A new general topology for cascaded multilevel inverters with reduced number of components based on developed H-bridgeIEEE Trans. Ind. Electron., 2014, 61, pp. 3932–3939.

[14] Gupta, K.K., Jain, S.: 'A novel multilevel inverter based on switched DC sourcesIEEE Trans. Ind. Electron., 2014, 61, pp. 3269–3278.

[15] Sadigh, A.K., Hosseini, S.H., Sabahi, M., Gharehpetian, G.B.: 'Double flying capacitor multicell converter based on modified phase-shifted pulsewidth modulation', IEEE Trans. Power Electron., 2010, 25, pp. 1517–1526.

[16] Dargahi, V., Abarzadeh, M., KhoshkbarSadigh, A., Dargahi, S.: 'Elimination of DC voltage sources and reduction of power switches voltage stress in stacked multicell converters: analysis, modeling, and implementation', Int. Trans. Electr. Energy Syst., 2014, 24, (5), pp. 653–676.

[17] Dargahi, V., Sadigh, A.K., Abarzadeh, M., Pahlavani, M.R.A., Shoulaie, A.: 'flying capacitors reduction in an improved double flying capacitor multicell converter controlled by a modified modulation method', IEEE Trans. Power Electron., 2012, 27, pp. 3875–3887.

[18] Sadigh, A.K., Dargahi, V., Abarzadeh, M., Dargahi, S.: 'Reduced DC voltage source flying capacitor multicell multilevel inverter: analysis and implementation', IET Power Electron., 2014, 7, pp. 439–450.

[19] Ajami, A., Oskuee, M.R.J., Mokhberdoran, A., Van den Bossche, A.: 'Developed cascaded multilevel inverter topology to minimise the number of circuit devices and voltage stresses of switches', IET Power Electron., 2014, 7, pp. 459–466.

[20] Kai-Ming, T., Wai-Lok, C.: 'Multi-level multi-output single-phase active rectifier using cascaded H-bridge converter', IET Power Electron., 2014, 7, pp. 784–794.

[21] Ajami, A., Shokri, H., Mokhberdoran, A.: 'Parallel switch-based chopper circuit for DC capacitor voltage balancing in diode-clamped multilevel inverter', IET Power Electron., 2014, 7, pp. 503–514.

[22] Marchesoni, M., Tenca, P.: 'Diode-clamped multilevel converters: a practicable way to balance DC-link voltages', IEEE Trans. Ind. Electron., 2002, 49, pp. 752–765.

[23] Adam, G.P., Williams, B.W.: 'New emerging voltage source converter for high-voltage application: hybrid multilevel converter with dc side H-bridge chain links', IET. Gener. Transm. Distrib., 2014, 8, pp. 765–773.

[24] Zha, X., Xiong, L., Gong, J., Liu, F.: 'Cascaded multilevel converter for medium-voltage motor drive capable of regenerating with part of cells', IET Power Electron., 2014, 7, pp. 1313–1320.

[25] Adil, E., Hassan, M., Abderrahim, B., Ahmed, A., Yassine, Z., Mohamed, A., Real Time Implementation of Sliding Mode Control for Induction Motor Drives Using dSPACE, (2015) International Review of Electrical Engineering (IREE) 10 (1).

[26] Mohamed, Y., S. Latha, Comparative Analysis of Multicarrier PWM Based Multilevel Z-Source Inverter Fed Induction Motor Drives with DTC for Different Modulation Indexes, (2014) International Review of Electrical Engineering (IREE), 9 (3).

[27] F. X. Edwin Deepak, Rajasekaran, V., R. Ranjitha, FPGA Implementation of Z-Source Multilevel Inverter Fed Induction Motor Drives, (2014) International Review of Electrical Engineering (IREE), 9 (4).

[28] Tejavathu Ramesh, Anup Kumar Panda, High Performance Direct Torque and Flux Control of Induction Motor Drive Using Fuzzy Logic Based Speed Controller, (2013) International Review of Electrical Engineering (IREE), 8 (2).

[29] Ponnambalam P., Praveenkumar M., Krishnamurthy K., MPC for Reduced Voltage Source Multicell Converter, (2014) International Review of Electrical Engineering (IREE), 9 (3).

[30] H. Merabet Boulouiha, A. Allali, M. Laouer, A. Tahri, M. Denaï, A. Draou. Direct torque control of multilevel SVPWM inverter in variable speed SCIG-based wind energy conversion system. Renewable Energy 80 (2015) 140–152.

[31] T. Meynardet H. Foch, « Multilevel converters and derived topologies for high power conversion », in *Proc. IEEE IECON*, vol. 1, pp. 21–26, 6–10 Nov. 1995.

[32] R. D. Lorenz and D. B. Lawson, A Simplified Approach to Continuous On-Line Tuning of Field-Oriented Induction Machine Drives, *IEEE Trans. On Industry application*, Vol. N°26, Issue/3, May-June 90.

[33] Merabet Boulouiha H, Allali A, Tahri A, Draou A, Denaï M. A simple maximum power point tracking based control strategy applied to a variable speed squirrel cage induction generator. J Renew Sustain Energy 2012; 4 (053124).

APPENDIX A

The parameters and values used in the simulation model are listed in Table A.1.

Table A.1 Parameters of the induction motor.

Induction motor	
Rated power, $P_{,n}$[kW]	2
Rated frequency,$f_{,n}$[Hz]	50
Stator resistance, R_s [Ω]	4.850
Stator leakage inductance, L_{ls} [mH]	16
Rotor resistance, R_r [Ω]	3.805
Rotor leakage inductance, L_{lr} [mH]	16
Mutual inductance, L_m [mH]	258
Inertia, J [kg.m^{-2}]	0.031
Viscous friction coefficient, f [N.m.sec.rad^{-1}]	0.00114

Number of pole pairs, p	2

Table A.2 Parameters of multicell-inverter.

DC side	
Capacity, C [μF]	5000
Switching frequency [kHz]	3

Table A.3: Parameters of indirect vector control IFOC.

IFOC control block	
Proportional gain speed controller, $K_{p\Omega}$	1
Integral gain speed controller, $K_{i\Omega}$	15.872

APPENDIX B: Dynamic model and IFOC strategy of the induction motor

The equivalent circuit of the induction motor is shown in Fig. ().

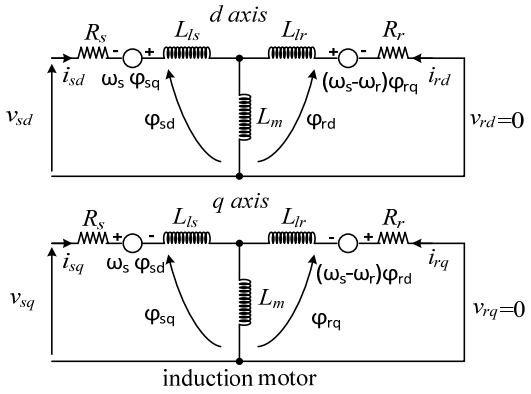

Fig. (B.1) Equivalent circuit of induction motor.

The relationships in the stator and rotor of the induction motor of Fig. (written in the Park system are:

Stator:

$$\begin{cases} v_{sd} = R_s i_{sd} + \dfrac{d\varphi_{sd}}{dt} - \omega_s \varphi_{sq} \\ v_{sq} = R_s i_{sq} + \dfrac{d\varphi_{sq}}{dt} + \omega_s \varphi_{sd} \end{cases} \qquad A.1)$$

Where v_{sd}, v_{sq} are the stator voltage components in the Park system, $\omega_s$is the synchronous speed of the generator, and $\varphi_{sd}, \varphi_{sq}$and i_{sd}, i_{sq} are respectively, the flux and stator current components in d and q axis of the Park frame. The fluxes are given by:

$$\begin{cases} \varphi_{sd} = L_s i_{sd} + L_m i_{rd} \\ \varphi_{sq} = L_s i_{sq} + L_m i_{rq} \end{cases} \qquad (A.2)$$

Rotor:

$$\begin{cases} v_{rd} = 0 = R_r i_{rd} + \dfrac{d\varphi_{rd}}{dt} - \omega_r \varphi_{rq} \\ v_{rq} = 0 = R_r i_{rq} + \dfrac{d\varphi_{rq}}{dt} + \omega_r \varphi_{rd} \end{cases} \tag{A.3}$$

The rotor voltages $v_{rd}$and $v_{rq}$are set to zero since the rotor is short-circuited, $\omega_r$is the rotor speed of the generator, and $\varphi_{rd}, \varphi_{rq}$and i_{rd}, i_{rq} are respectively the flux and rotor current components in *d* and *q* axis of the Park frame. The fluxes are given by:

$$\begin{cases} \varphi_{rd} = L_m i_{sd} + L_r i_{rd} \\ \varphi_{rq} = L_m i_{sq} + L_r i_{rq} \end{cases} \tag{A.4}$$

The dynamic model of an induction machine is described by the following equations written in the dq synchronous reference frame:

$$\begin{cases} \dfrac{di_{sd}}{dt} = -\left(\dfrac{1}{T_s\sigma} + \dfrac{(1-\sigma)}{T_r\sigma}\right) i_{sd} + \omega_s i_{sq} + \dfrac{(1-\sigma)}{T_r L_m \sigma}\varphi_{rd} + \dfrac{(1-\sigma)}{L_m\sigma}\omega_r\varphi_{rq} + \dfrac{1}{L_s\sigma}v_{sd} \\ \dfrac{di_{sq}}{dt} = -\omega_s i_{sd} - \left(\dfrac{1}{T_s\sigma} + \dfrac{(1-\sigma)}{T_r\sigma}\right) i_{sq} - \dfrac{(1-\sigma)}{L_m\sigma}\omega_r\varphi_{rd} + \dfrac{(1-\sigma)}{T_r L_m\sigma}\varphi_{rq} + \dfrac{1}{L_s\sigma}v_{sq} \\ \dfrac{d\varphi_{rd}}{dt} = \dfrac{L_m}{T_r} i_{sd} - \dfrac{1}{T_r}\varphi_{rd} + \omega_{slip}\varphi_{rq} \\ \dfrac{d\varphi_{rq}}{dt} = \dfrac{L_m}{T_r} i_{sq} - \omega_{slip}\varphi_{rd} - \dfrac{1}{T_r}\varphi_{rq} \\ T_{em} = p\dfrac{3}{2}\dfrac{L_m}{L_r}\left(\varphi_{rd} i_{sq} - \varphi_{rq} i_{sd}\right) \\ T_{em} - T_r = J\dfrac{d\Omega_r}{dt} + f\Omega_r \end{cases} \tag{A.5}$$

Where: $\omega_r = p\Omega_r$; $\omega_{slip} = [\omega_s - \omega_r]$; $T_r = \frac{L_r}{R_r}$; $T_s = \frac{L_s}{R_s}$

With σ is the coefficient of dispersion and is given by

$$\sigma = 1 - \frac{L_m^2}{L_s L_r} \tag{A.6}$$

Where T_{em} is the electromagnetic torque [N·m] and $T_m$denotes the mechanical torque produced by the load [N·m]. The major aim of the vector control of induction motors is, as in DC machines, to separately control the torque and the flux; this is done by using a *d-q* rotating reference frame synchronously with the rotor flux space vector [32] as shown in fig. 1, the *d* axis is aligned with the rotor flux space vector. Under this condition we have:$\varphi_{rq} = 0$and$\varphi_{rd} = \varphi_r$

Thus, the dynamic equations (A.5) yield:

$$\begin{cases} v_{sd} = R_s i_{sd} - \omega_s L_s \sigma i_{sq} \\ v_{sq} = \omega_s L_s i_{sd} + R_s i_{sq} \\ \varphi_r = L_m i_{sd} \Rightarrow \ i_{sd} = \dfrac{\varphi_r}{L_m} \\ \omega_{slip} = \dfrac{L_m}{T_r}\dfrac{i_{sq}}{\varphi_r} \\ T_{em} = \ p\dfrac{3}{2}\dfrac{L_m}{L_r}\varphi_{rd} i_{sq} \\ T_{em} - T_r = J\dfrac{d\Omega_r}{dt} + f\Omega_r \end{cases} \tag{A.7}$$

APPENDIX C: Design of the PI and FLC controllers

C. 1 PI controller

Speed controller can determine the electromagnetic torque reference in order to maintain the same speed. The speed can be controlled using a PI controller.

The transfer function of the mechanical speed of the induction motor is given by

$$\frac{\Omega_r}{T_{em}} = \frac{1}{Js + f} = \frac{G_\Omega}{s + p_\Omega} \tag{C.1}$$

where $G_\Omega = \frac{1}{J}$ and $p_\Omega = \frac{f}{J}$ are respectively, the static gain and the pole of the transfer function of the mechanical speed of the asynchronous generator.

The closed-loop transfer function is

$$T_{CL}(s) = \frac{G_\Omega\left[K_{p_\Omega} s + K_{i_\Omega}\right]}{s^2 + \left[G_\Omega K_{p_\Omega} + p_\Omega\right]s + G_\Omega K_{i_\Omega}} \tag{C.2}$$

The controller parameters can be determined using pole placement. Let the desired closed-loop poles be

$$s_{1,2} = -\sigma_c \pm j\omega_n\sqrt{1 - \xi^2} = \gamma(-1 \pm j) \tag{C.3}$$

The poles are selected to improve the closed-loop response by three-fold with regard to the open-loop system. Solving for the PI controller's parameter [33]

$$\begin{cases} K_{p_\Omega} = \frac{2\gamma - p_\Omega}{G_\Omega} \\ K_{i_\Omega} = \frac{2\gamma^2}{G_\Omega} = 2\gamma^2 J \end{cases} \tag{C.4}$$

C. 2 FLC controller

The following structure shows the diagram of an FLC controller:

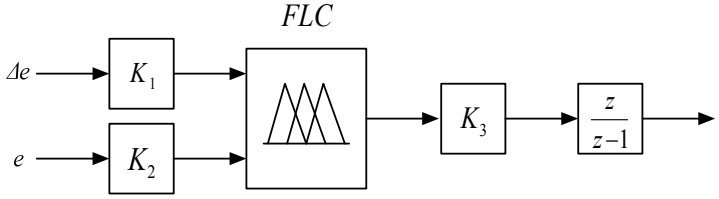

Fig. C.1 Scheme of the FLC controller

The input variables are the error and its derivative

$$\begin{cases} e(k) = \omega_{ref} - \omega_m \\ \Delta e(k) = e(k) - e(k-1) \end{cases} \quad (C.5)$$

The input and output universe of discourse are normalized [-1.1]. Thus there should be adaptation gains for the desired dynamics, but there is no systematic technique for the determination of these gains, and hence a trial and error procedure is used. The selected membership functions have a trapezoidal and triangular ends in the universe of discourse (Fig. (C.2)).

The defuzzification is based on the center of gravity method. For the membership functions were chosen for each variable triangular and trapezoidal shape as shows in Fig.(C.2).

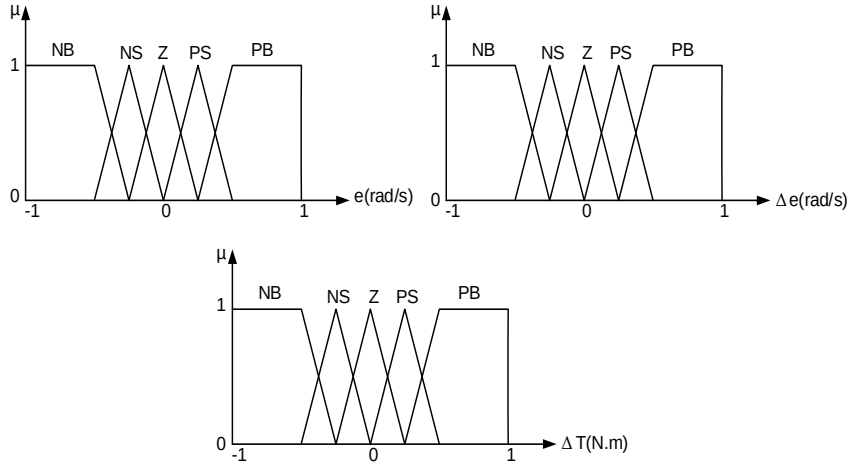

Fig. C.2 The inputs and output membership function

Where NB = Negative Big, NS = Negative Small, Z = Approximalely zero, PS = Positive Small, PB = Positive Big.

Table C.1: FLC rules.

e / Δe	**GN**	**PN**	**Z**	**PP**	**GP**
GN	GN	GN	GN	PN	Z
PN	GN	GN	PN	Z	PP
E	GN	PN	Z	PP	GP
PP	PN	Z	PP	GP	GP
GP	E	PP	GP	GP	GP

Fuzzy command manipulates language knowledge and has a wealth of options for the shape of the membership functions, the type of fuzzification and defuzzification and type inference.

APPENDIX D: Modeling of the multicellular inverter by N-cells

The N-cell instantaneous model connected in series (Fig. D.1) is presented in the following.

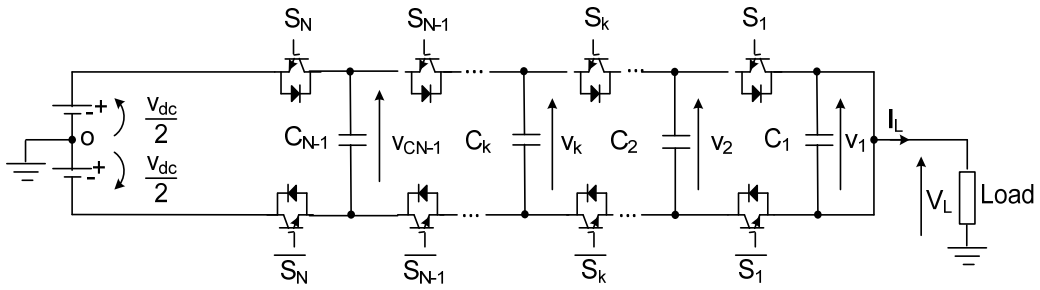

Fig. D.1 General structure of a single arm of a multicell inverter.

The setting in equation of this connection considers local variations in the voltage of each floating capacitor. These variations depend on the output current i and the difference between the duty cycles of the adjacent switching cells (k, k -1) in each capacitor k.

$$\frac{dv_{C_1}(t)}{dt} = \frac{i_L(t)}{C}(S_2 - S_1) \tag{D.1}$$

$$\frac{dv_{C_k}(t)}{dt} = \frac{i_L(t)}{C}(S_{k+1} - S_k) \tag{D.2}$$

$$\frac{dv_{C_{n-1}}(t)}{dt} = \frac{i_L(t)}{C}(S_{k+1} - S_k) \tag{D.3}$$

The representation of this model in a matrix form is presented below.

$$\frac{d}{dt}\begin{pmatrix} v_{C_1}(t) \\ v_{C_2}(t) \\ v_{C_3}(t) \\ \vdots \\ v_{C_{n-1}}(t) \end{pmatrix} = \frac{1}{C}\begin{pmatrix} -i_L(t) & i_L(t) & 0 & \cdots & 0 \\ 0 & -i_L(t) & i_L(t) & \cdots & 0 \\ 0 & 0 & -i_L(t) & \cdots & 0 \\ \vdots & \vdots & \vdots & \vdots & \vdots \\ 0 & 0 & \ldots & -i_L(t) & i_L(t) \end{pmatrix}\begin{pmatrix} S_1 \\ S_2 \\ S_3 \\ \vdots \\ S_N \end{pmatrix} \tag{D.4}$$

To ensure normal operation, it is indispensable to make certain a balanced distribution of the floating voltages $v_{Cj,k} = kv_{dc}/N$ (where$j$=abccorresponding the three phase). The N-cell output voltage $v_{Cj,k}$ can be determined by: $\left(\frac{v_{dc}}{N}, \ldots, (N-1)\frac{v_{dc}}{N}, v_{dc}\right)$

$$\begin{bmatrix} v_{La} \\ v_{Lb} \\ v_{Lc} \end{bmatrix} = \begin{bmatrix} 2 & -1 & -1 \\ -1 & 2 & -1 \\ -1 & -1 & 2 \end{bmatrix}\begin{bmatrix} v_{AM} \\ v_{BM} \\ v_{CM} \end{bmatrix} \tag{D.5}$$

With:

$$\begin{cases} v_{aO} = v_{sa} - \dfrac{v_{dc}}{2} \\ v_{bO} = v_{sb} - \dfrac{v_{dc}}{2} \\ v_{cO} = v_{sc} - \dfrac{v_{dc}}{2} \end{cases} \tag{D.6}$$

The output voltage v_{si} corresponds to the addition of terminal voltages of the switches.

$$v_{s_i} = \sum_{k=1}^{N} v_{j,k} = \sum_{k=1}^{N} S_{j,k}\left(v_{Cj,k} - v_{Cj,k-1}\right) \tag{D.7}$$

through: $v_{C_{j,N}} = \frac{v_{dc}}{2}$ and $v_{C_{j,0}} = 0$

So

$$\begin{bmatrix} v_{La} \\ v_{Lb} \\ v_{Lc} \end{bmatrix} = \frac{1}{3}\begin{bmatrix} 2 & -1 & -1 \\ -1 & 2 & -1 \\ -1 & -1 & 2 \end{bmatrix}\begin{bmatrix} \sum_{k=1}^{N} S_{a,k}\left(v_{Ca,k} - v_{Ca,k-1}\right) \\ \sum_{k=1}^{N} S_{b,k}\left(v_{Cb,k} - v_{Cb,k-1}\right) \\ \sum_{k=1}^{N} S_{jc,k}\left(v_{Cc,k} - v_{Cc,k-1}\right) \end{bmatrix} \tag{D.8}$$

The variations of the floating voltages $v_{Cj,k}$ is a function of the current I_{lj}, which in rotate depends on the state of the adjacent cells $Cel_{j,k+1}$, $Cel_{j,k}$ and the load current i_{Lj}. The current i_{Cj} is a function of the control signals of switches $S_{j,k+1}$ and $S_{j,K}$.